








Models of Learning to Classify X-ray Images for the Detection of Pneumonia using Neural Networks

A. A. Saraiva^{2,3} ^a, D. B. S. Santos² ^b, Nator Junior C. Costa² ^c, Jose Vigno M. Sousa^{1,2} ^d,
N. M. Fonseca Ferreira^{4,5} ^e, Antonio Valente^{3,6} ^f and Salviano Soares⁷ ^g

¹University Brazil, São Paulo, Brazil

²UESPI-University of State Piauí, Piripiri, Brazil

³School of Science and Technology, University of Trás-os-Montes and Alto Douro, Vila Real, Portugal

⁴Department of Electrical Engineering, Institute of Engineering of Coimbra, Coimbra, Polytechnic Institute, Portugal

⁵Knowledge Engineering and Decision-Support Research Center (GECAD) of the Institute of Engineering, Polytechnic Institute of Porto, Portugal

⁶NESEC-TEC Technology and Science, Campus da FEUP, Rua Dr. Roberto Frias 378, 4200-465 Porto, Portugal

⁷University of Trás-os-Montes and Alto Douro, Vila Real, Portugal

Keywords: Pneumonia, CNN, MLP, Classification, k-Fold, Chest-X-Ray.

Abstract: This article describes a comparison of two neural networks, the multilayer perceptron and Neural Network, for the detection and classification of pneumonia. The database used was the Chest-X-Ray data set provided by (Kermany et al., 2018) with a total of 5840 images, with two classes, normal and with pneumonia. To validate the models used, cross-validation of k-fold was used. The classification models were efficient, resulting in an average accuracy of 92.16% with the Multilayer Perceptron and 94.40% with the Convolution Neural Network.

1 INTRODUCTION

According to the World Health Organization report, pneumonia killed 920,136 children under 5 years old in 2015, accounting for 16% of all pediatric deaths (Organization, 2015). Pneumonia is an acute respiratory infection that affects the lungs and can be caused by bacteria, viruses or fungi.

Pneumonia is the leading cause of infectious disease-related mortality in Western countries. However, the diagnosis of pneumonia is usually difficult in the emergency setting, since clinical, biological and imaging signs are not specific.


The unavailability of low-cost (Saraiva et al., 2018a), field-deployable rapid diagnostic technol-


ogy (Saraiva et al., 2018d), (Saraiva et al., 2018g), (Saraiva et al., 2018e), (Marques et al., 2018), is one of the major challenges in combating pneumonia mortality. Currently, there is an absence of gold standard for the diagnosis of pneumonia, even in hospitals (Kosasih et al., 2015).


In this way, it inspired the design of an image classifier (Saraiva et al., 2018b), in order to diagnose patients with pneumonia in an automated and fast way. The method selected and implemented constitutes a classification of chest X-ray images of patients, from which it is possible to identify whether or not the patient has pneumonia. For the classification, the Dataset Chest X-Ray was used in the total 5216 images provided by (Kermany et al., 2018).


The classification stage consists of two sub-stages, where in the first classification is performed by an artificial intelligence, consisting of a deep learning known as Convolutional Neural Networks (CNN) (Ponzio et al., 2018), (Mabaso et al., 2018), (Lisowska et al., 2017), the second is to perform the classification with a deep learning Multilayer Perceptron (MLP). The method covered ensures a robust


^a  <https://orcid.org/0000-0002-3960-697X>


^b  <https://orcid.org/0000-0003-4018-242X>

^c  <https://orcid.org/0000-0001-5636-424X>

^d  <https://orcid.org/0000-0002-5164-360X>

^e  <https://orcid.org/0000-0002-2204-6339>

^f  <https://orcid.org/0000-0002-5798-1298>

^g  <https://orcid.org/0000-0001-5862-5706>

coverage in image recognition (Saraiva et al., 2018f), (Saraiva et al., 2018h), under certain assumptions that will be clarified throughout the text.

The document is divided into 7 sections, in which section 2 is characterized by the contextualization of the work. It follows the methodology applied and the validation metrics in section 3. The description of the database is in section 4, the results after the application of the proposal in section 5, section 6 deals with the discussions and conclusion in the section 7.

2 CONTEXTUALIZATION OF WORK

It is possible to observe in the work of (Lakhani and Sundaram, 2017), the effectiveness of the use of deep convolutional neural networks (DCNNs) for the detection of Tuberculosis through four sets of HIPAA data and two different DCNNs, AlexNet and GoogLeNet.

(Rajpurkar et al., 2017), CheXNet is a 121-layer convolutional neural network trained in ChestX-ray14, capable of detecting pneumonia by checking thoracic radiographs, which when compared to the performance of four practicing academic radiologists, CheXNet is able to overcome professionals.

In (Becker et al., 2018), evaluates the viability of using Deep Learning and classification of pathological patterns in a set of digital photographs of chest X-ray images of patients with tuberculosis, using diagnoses of the same it was possible to analyze pathological patterns in classes: cavity, consolidation, stroke, interstitial changes, miliary pattern or normal examination.

(Xue et al., 2018), demonstrates a method of sexual identification through frontal thoracic radiographs, motivated by the need to determine missing gender information in some datasets employing the Deep Learning-based convolutional neural network (CNN) technique and learning transfer, with an accuracy of 86, 6 % and ROC area with 0.932 for 5-fold cross-validation.

According to Becker, (Hooda et al., 2017) It points out a potential method for the detection of tuberculosis using deep learning, which classifies RXT images into two categories, that is, normal and abnormal. Using the CNN architecture with 7 convoluted layers and 3 fully connected layers.

(Vajda et al., 2018), consists of an automatic analysis and classification of chest radiographs can be used as a reliable alternative to more sophisticated and technologically demanding methods (eg culture or smear analysis), with a fully automatic TB screen-

ing system processing the CXRs of thorax) and applying image preprocessing techniques to improve image quality, followed by adaptive segmentation based on model selection.

The study of (Sivaramakrishnan et al., 2017), aims to visualize salient network activations in a Deep Learning model based on Convolutional Neural Network (CNN), applied to the challenge of the chest X-ray screening. Computer-aided detectio software using machine learning approaches was developed to analyze CXRs for abnormalities in order to reduce delays in configurations with limited resources.

3 MATERIALS AND METHODS

In This Section, it will be presented the structure of the adopted systems, to resolve the classification of pneumonia, classifying them as normal or with pneumonia, will also be presented the entire structure of the algorithms as well as the evaluation metrics.

3.1 Structure of the System

In Figure 1 it is possible to visualize the structure of the system, in which the steps consists of the following order: acquisition of the images, soon after k-fold is used in order to divide the training and test data. Preprocessing is about normalizing the data, ie past grayscale images and all pixels are divided by 255 to transform them into floating points. Finally, the classification of the images with the two proposed learning models is done.

Two learning models, neural networks known as CNN and MLP, are described, described in the sections below. In Figures 3 and 5 it is possible to observe the structure of both neural networks. In the step of predicting test data the input of the test images separated by the k-fold algorithm is performed and the accuracy is collected. The process is repeated 5 times, changing the test and training images following the calculation of k-fold.

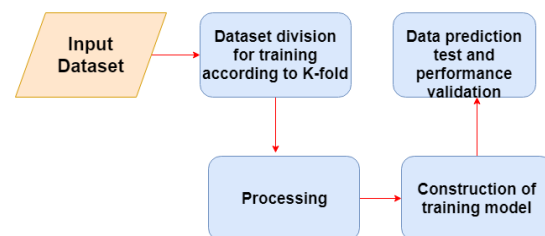


Figure 1: Construct, training and validate of the model.

CNN and MLP processing was performed using a 6 GB NVIDIA GTX 1060 video card, which has 1280

CUDA cores and an Intel Core i7 processor with 12 Gigabytes of RAM, although most of the processing is done per video card, since CNN and MLP can run on GPUs, if available.

In Figure 2, one can observe the operation of the models soon after the training, this process consists of the input of the image, then the pre-processing is done and finally the image is predicted with the model (CNN or MLP), where the image is classified as normal or pneumonia.

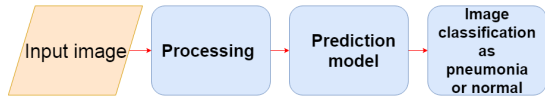


Figure 2: Image input and prediction.

3.2 MLP

MLP is an artificial feedforward neural network class, consisting of at least three node layers, except for the input nodes, each node is a neuron that uses a nonlinear activation function (Tang et al., 2016). The MLP uses a supervised learning technique called backpropagation for training (Pham et al., 2017).

Its multiple layers and non-linear activation distinguish MLP from a linear perceptron in this way one can distinguish data that are not linearly separable. (Pham et al., 2017). In Figure 3 a network composed of five layers is presented, one layer being input, three hidden layers with the function Rectified Linear Unit (ReLU) and an output layer with the function Softmax.

In the equations 1 and 2 it is possible to verify the function ReLU, responsible for calculating the output of a node according to its input in a neuron.

$$f(x) = x^+ = \max(0, x) \quad (1)$$

$$f(x) = \begin{cases} 0 & \text{for } x < 0 \\ x & \text{for } x \geq 0 \end{cases} \quad (2)$$

In the equation 3 it is possible to see the softmax function, where z is an input vector for output layer, in this work if there are 2 output classes, then z is a vector of two elements. E_j indexes the output units.

$$\sigma(\mathbf{z})_j = \frac{e^{z_j}}{\sum_{k=1}^K e^{z_k}} \quad (3)$$

In the 4 equation we have the function responsible for calculating the loss, called a cross-entropy, where D represents the distance and receives two lists, p and q . where the loss is calculated.

$$D(p, q) = - \sum_x p(x) \log q(x). \quad (4)$$

The figure 3, consists of the structure of the model of the MLP used, at the beginning one has the input layer where the images are multiplied by the weights and added to the bias, later the hidden layers of the network are defined, three layers, with ReLUs activation functions. The first layer has 32 units the second 64 and the third 128, in the layer of output, last layer, the softmax function is used.

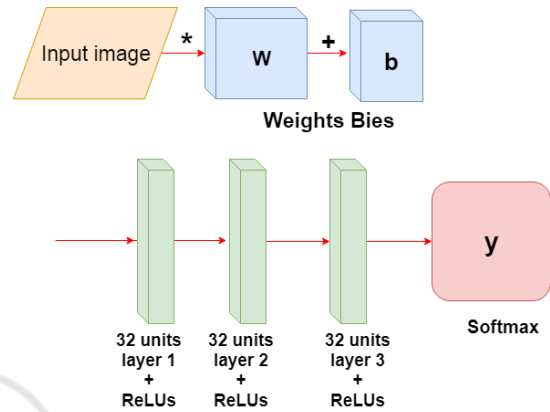


Figure 3: Construction of the MLP training model.

3.3 CNN

CNNs are similar to traditional neural networks, both are composed of neurons that have weights and bias that need to be trained. Each neuron receives some inputs, applies the scalar product of inputs and weights in addition to a non-linear function (Chen et al., 2017).

A CNN consists of a sequence of layers Figure 5, in addition to the input layer, which usually consists of an image with width and height, there are three main layers: convolutional layer, Pooling layer and fully connected layer. In addition, after a convolutional layer it is common an activation layer normally a linear rectification unit function (ReLU) equations 1, 2. These layers, when sequenced (or stacked), form an architecture of a CNN (Salamon and Bello, 2017).

3.3.1 Convolutional Layer

This layer is composed of a set of filters (kernels) capable of learning according to a training (Ustinova et al., 2017). The kernels are small matrices that in this case was used the size 3x3 to obtain a better precision in the time to go through the matrix of the images, composed by real values that can be interpreted as weights.

Given a two-dimensional image, I , and a small array, K of size $h \times w$ (kernel), the convoked image, $I * K$, is calculated by overlapping the kernel at the top

of the image of all possible shapes, and recording the sum of the elementary products between the image and the kernel equation 5.

$$(I * K)_{xy} = \sum_{i=1}^h \sum_{j=1}^w K_{ij} \cdot I_{x+i-1, y+j-1} \quad (5)$$

The kernels are convolved with the input data to get a feature map. These maps indicate regions in which specific features in relation to kernels. The actual values of the kernels change over the course of the training causing the network to learn to identify significant regions to extract characteristics from the data set (Maggiore et al., 2017), so each filter results in an output of a three-dimensional array. In the convolution results matrices the ReLU activation function, equations 1, 2 are applied. in each element of the convolution result.

3.3.2 Pooling Layer

After a convolution layer exists a pooling layer, the pooling technique is used to reduce the spatial size of the resulting convolution matrices, according to the figure 4. Consequently, this technique reduces the amount of parameters to be learned in the network, contributing to the control of overfitting, ie avoiding the condition when a trained model works very well in training data, but does not work very well in test data (Yu et al., 2017).

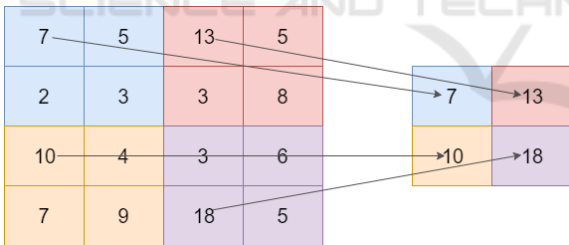


Figure 4: Example max-pooling with a 2x2 image.

The maximum pool operation reduces the size of the resource map, this operation can be described by the equation 6. Let S be the value of the passed and $Q \times Q$ the shape of the feature map before the maximum grouping and p determines the clustering max-pooling size (Havaei et al., 2017). The output of the max-pooling operation would be $D \times D$ size.

$$D = (Q - p) / S + 1 \quad (6)$$

3.3.3 Fully Connected Layer

The fully connected layer comes after a convolutional or pooling layer, it is necessary to connect each element of the convolution output matrices to an input

neuron. The output of the convolutional and pooling layers represent the characteristics extracted from the input image.

The last layer of the network uses softmax as the activation function, equation 3. This function receives a vector of values as input and produces the

The technique known as dropout is also used in the fully connected layer to reduce training time and avoid overfitting. This technique consists in randomly removing a certain percentage of neurons from a layer at each training iteration, re-adding them to the next iteration (Kovács et al., 2017).

3.3.4 CNN Architecture

In Figure 5 the CNN architecture is displayed, it has three convolution layers and the last one is fully connected, the input of the network receives a 150x150 pixel image, each convolution layer has the ReLU activation function. For the convolution kernel, the 3x3 size was adopted, because this way it is possible to have a greater precision in the time to go through the entire image.

After each convolutional layer a Max-pooling layer is used, in this way the size of the matrices resulting from the convolution is reduced. With this layer it is possible to reduce the amount of parameters that will be learned by the network, this way it is done overfitting control.

In the fully connected layer the softmax activation function is used, this function is responsible for making the probabilistic distribution of the input image belong to each of the classes in which the network was trained. To reduce the training time and to avoid

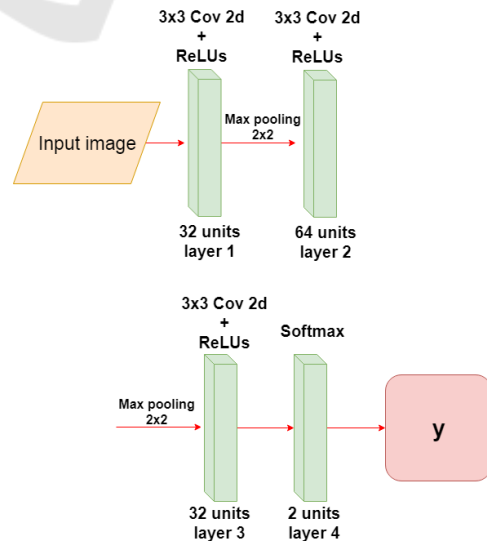


Figure 5: Construction of the CNN training model.

overfitting is used dropout in the layer, ie it is randomly removed at each training interaction, a certain percentage of the neurons of a layer, re-adding them in the following iteration.

4 DESCRIPTION OF THE DATASET

The set of images contains 5863 X-ray (JPEG) images and 2 categories (Pneumonia / Normal) provided by the (Wang et al., 2017). It is possible to visualize in the figures 6 e 7.

Chest x-ray images (anteroposterior) were selected from pediatric patients aged one to five years. The image comes from Guangzhou Women and Children's Medical Center. All chest X-ray images were performed as part of the routine clinical care of the patients (Wang et al., 2017).

The dataset still has quality control, where illegible and low-quality images have been removed. The diagnosis was classified by two specialist doctors and checked by a third expert in order to extinguish the errors (Wang et al., 2017).

The dataset consists of 5863 images, being 1575 images of normal patients and 4288 of patients with



Figure 6: Normal.

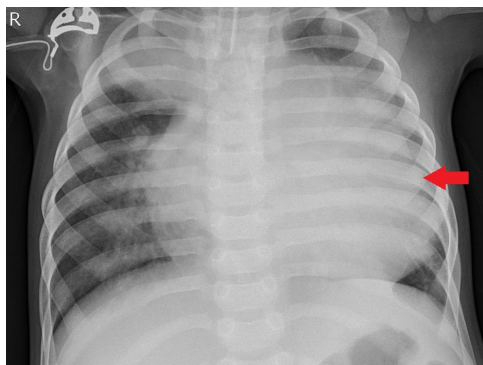


Figure 7: Pneumonia.

pneumonia. To create the learning model, it was necessary to balance the images.

Pneumonia causes pulmonary consolidation, this means that the pulmonary alveoli are filled with inflammatory fluid, this fluid replaces the air in the alveoli, so that the affected part of the lung does not contain air (Iorio et al., 2018). In the radiographic, pulmonary consolidation corresponds to an opacity (whitish area).

The identification of the existence of pneumonia is based on the opacities of the radiography, that is, the radiograph shows the darker part near the spine that corresponds to the bronchi (Kunz et al., 2018). The air contained in the bronchi gives this color to the radiograph, while the outside of the lung is lighter (opaque) because the alveoli are filled with fluid Figure 7.

5 METRICS OF THE EVALUATION

5.1 Cross Validation

Cross-validation is an evaluation technique on the ability of generalization models, from a dataset, is widely used in problems where the object is the modeling and prediction (Vehtari et al., 2017). With this it is possible to estimate how precise the model is, that is, its accuracy with data that it does not know.

The k-fold cross-validation method consists of dividing the total set into k subsets of the same size, one subset is used for testing, and the other $k-1$ subsets for training. This process is repeated by k times, if circularly changing the subset of tests (Grimm et al., 2017).

The final precision of the model is estimated by equation 7, at where Ac_f is the sum of the differences between the actual value y_i and the predicted value \hat{y}_i and k is the amount of k-fold divisions. With this it is possible to infer the generalization capacity of the network.

$$Ac_f = \frac{1}{k} \sum_{i=1}^k (y_i - \hat{y}_i) \quad (7)$$

5.2 Confusion Matrix

As a statistical tool we have the confusion matrix that provides the basis for describe the accuracy of the classification and characterize the errors, helping refine the ranking (Saraiva et al., 2018c).

The measures derived from the confusion matrix are: the total accuracy being that chosen by the

Table 1: Table of MLP Network Interaction Results Table.

Interaction	Accuracy	True Negative	False negative	True Positive	False positive
1	92.38 %	277	38	305	10
2	93.68 %	267	25	325	13
3	90.15 %	286	23	282	39
4	91.90 %	322	13	257	38
5	92.69 %	299	25	285	21
Average	92.16 %	290.2	24.8	290.9	24.2

Table 2: Table of CNN network interaction results.

Interaction	Accuracy	True Negative	False negative	True Positive	False positive
1	94.44 %	286	23	309	12
2	94.76 %	298	18	299	15
3	95.07 %	286	17	313	14
4	94.28 %	303	14	291	22
5	93.49 %	316	14	273	27
Average	94.40 %	297.8	17.2	297	18

present work, accuracy of individual class, producer precision, user precision and Kappa index, among others. The total accuracy is calculated by dividing the sum of the main diagonal of the error matrix x_{ii} , by the total number of samples collected n . According to the equation 8.

$$T = \frac{\sum_{i=1}^a x_{ii}}{n} \quad (8)$$

6 RESULTS

In this section will be presented the performance results of both neural networks. The metrics used to evaluate the results are: Mean of cross validation accuracy, mean number of false positive and false negative, of both models.

In the table 2 the results obtained by the MLP network are presented, the data are: iteration, test data accuracy, true negative, false negative, true positive, false positive. The mean accuracy obtained by the

network was 92.16 %, with an average of 24.2 false positive, 24.8 false negative.

In the figure 8 it is possible to verify the ROC curve and the error precision curve in the figure 9 referring to the interaction 5 of the table 2, in it is possible to verify the specificity and sensitivity of the model. In the figures 10 and 11 the confusion matrices for iteration 5 of the table 2.

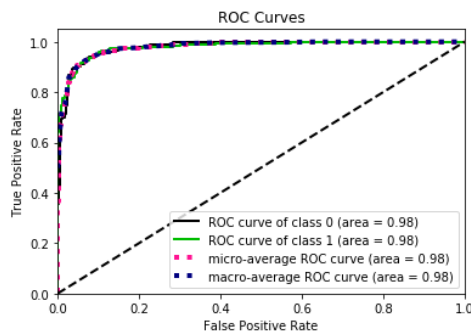


Figure 8: Curve roc MLP interaction 5(table 2).

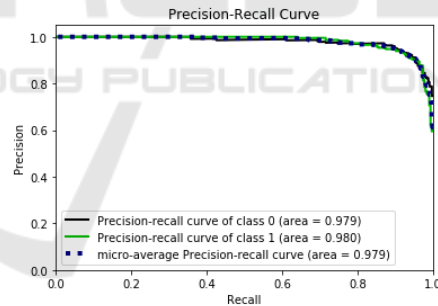


Figure 9: Precision Recall curve interaction 5(table 2).

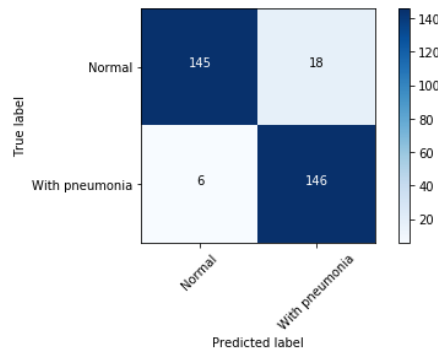


Figure 10: Confusion matrix, without normalization, MLP interaction 5 (table 2).

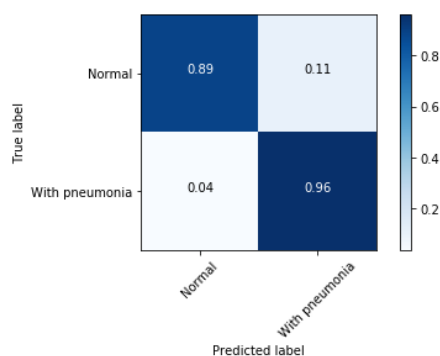


Figure 11: Normalized confusion matrix, interaction 5 (table 2).

7 CONCLUSIONS

In this work we have demonstrated comparative of two classification models, for the diagnosis of pneumonia. For the validation of the models, cross validation was performed, where it is possible to verify the generalization capacity. The artificial neural networks used were: CNN and MLP. The proposed classification models proved to be efficient in classification, with CNN obtaining 94.40 % accuracy and MLP with 92.16%.

As future work, it is suggested to increase the number of diseases that are also diagnosed through radiographic thoracic, and to use other classifiers.

ACKNOWLEDGMENTS

This work is financed by National Funds through the FCT - Fundação para a Ciência e a Tecnologia (Portuguese Foundation for Science and Technology) as part of project UID/EEA/00760/2019.

REFERENCES

- Becker, A., Blüthgen, C., Sekaggya-Wiltshire, C., Castelnovo, B., Kambugu, A., Fehr, J., Frauenfelder, T., et al. (2018). Detection of tuberculosis patterns in digital photographs of chest x-ray images using deep learning: feasibility study. *The International Journal of Tuberculosis and Lung Disease*, 22(3):328–335.
- Chen, Y.-H., Krishna, T., Emer, J. S., and Sze, V. (2017). Eyeriss: An energy-efficient reconfigurable accelerator for deep convolutional neural networks. *IEEE Journal of Solid-State Circuits*, 52(1):127–138.
- Grimm, K. J., Mazza, G. L., and Davoudzadeh, P. (2017). Model selection in finite mixture models: A k-fold cross-validation approach. *Structural Equation Modeling: A Multidisciplinary Journal*, 24(2):246–256.
- Havaei, M., Davy, A., Warde-Farley, D., Biard, A., Courville, A., Bengio, Y., Pal, C., Jodoin, P.-M., and Larochelle, H. (2017). Brain tumor segmentation with deep neural networks. *Medical image analysis*, 35:18–31.
- Hooda, R., Sofat, S., Kaur, S., Mittal, A., and Meriaudeau, F. (2017). Deep-learning: a potential method for tuberculosis detection using chest radiography. In *Signal and Image Processing Applications (ICSIPA), 2017 IEEE International Conference on*, pages 497–502. IEEE.
- Iorio, G., Capasso, M., Prisco, S., De Luca, G., Mancusi, C., Laganà, B., Piscopo, M. A., and Comune, V. (2018). Lung ultrasound findings undetectable by chest radiography in children with community-acquired pneumonia. *Ultrasound in medicine & biology*.
- Kermany, D., Zhang, K., and Goldbaum, M. (2018). Labeled optical coherence tomography (oct) and chest x-ray images for classification. *Structural Equation Modeling: A Multidisciplinary Journal*.
- Kosasih, K., Abeyratne, U. R., Swarnkar, V., and Triasih, R. (2015). Wavelet augmented cough analysis for rapid childhood pneumonia diagnosis. *IEEE Trans. Biomed. Engineering*, 62(4):1185–1194.
- Kovács, G., Tóth, L., Van Compernelle, D., and Ganapathy, S. (2017). Increasing the robustness of cnn acoustic models using autoregressive moving average spectrogram features and channel dropout. *Pattern Recognition Letters*, 100:44–50.
- Kunz, W. G., Patzig, M., Crispin, A., Stahl, R., Reiser, M. F., and Notohamiprodo, M. (2018). The value of supine chest x-ray in the diagnosis of pneumonia in the basal lung zones. *Academic radiology*.
- Lakhani, P. and Sundaram, B. (2017). Deep learning at chest radiography: automated classification of pulmonary tuberculosis by using convolutional neural networks. *Radiology*, 284(2):574–582.
- Lisowska, A., Beveridge, E., Muir, K., and Poole, I. (2017). Thrombus detection in ct brain scans using a convolutional neural network. In *Proceedings of the 10th International Joint Conference on Biomedical Engineering Systems and Technologies - Volume 2: BIOIMAGING, (BIOSTEC 2017)*, pages 24–33. INSTICC, SciTePress.
- Mabaso, M., Withey, D., and Twala, B. (2018). Spot detection in microscopy images using convolutional neural network with sliding-window approach. In *Proceedings of the 11th International Joint Conference on Biomedical Engineering Systems and Technologies - Volume 2: BIOIMAGING, (BIOSTEC 2018)*, pages 67–74. INSTICC, SciTePress.
- Maggiori, E., Tarabalka, Y., Charpiat, G., and Alliez, P. (2017). Convolutional neural networks for large-scale remote-sensing image classification. *IEEE Transactions on Geoscience and Remote Sensing*, 55(2):645–657.
- Marques, J. F., das Chagas, Fontenele, A. A., Costa, J. V. M., De Araujo, N. F., and Valente, A. (2018). Manipulation of bioinspiration robot with gesture recognition through fractional calculus. *IEEE LARS 2018 – 15th Latin American Robotics Symposium*.

- Organization, W. H. (2015). *The Selection and Use of Essential Medicines: Report of the WHO Expert Committee, 2015 (including the 19th WHO Model List of Essential Medicines and the 5th WHO Model List of Essential Medicines for Children)*. Number 994. World Health Organization.
- Pham, B. T., Bui, D. T., Prakash, I., and Dholakia, M. (2017). Hybrid integration of multilayer perceptron neural networks and machine learning ensembles for landslide susceptibility assessment at himalayan area (india) using gis. *Catena*, 149:52–63.
- Ponzio, F., Macii, E., Ficarra, E., and Cataldo, S. D. (2018). Colorectal cancer classification using deep convolutional networks. In *Proceedings of the 11th International Joint Conference on Biomedical Engineering Systems and Technologies - Volume 2: BIOIMAGING, (BIOSTEC 2018)*, pages 58–66. INSTICC, SciTePress.
- Rajpurkar, P., Irvin, J., Zhu, K., Yang, B., Mehta, H., Duan, T., Ding, D., Bagul, A., Langlotz, C., Shpanskaya, K., et al. (2017). Chexnet: Radiologist-level pneumonia detection on chest x-rays with deep learning. *arXiv preprint arXiv:1711.05225*.
- Salamon, J. and Bello, J. P. (2017). Deep convolutional neural networks and data augmentation for environmental sound classification. *IEEE Signal Processing Letters*, 24(3):279–283.
- Saraiva, A., Barros, M., Nogueira, A., Fonseca Ferreira, N., and Valente, A. (2018a). Virtual interactive environment for low-cost treatment of mechanical strabismus and amblyopia. *Information*, 9(7):175.
- Saraiva, A., Ferreira, N., and Valente, A. (2018b). New bioinspired filter of dicom images.
- Saraiva, A., Melo, R., Filipe, V., Sousa, J., Ferreira, N. F., and Valente, A. (2018c). Mobile multirobot manipulation by image recognition.
- Saraiva, A., Miranda de Jesus Castro, F., Ferreira, N., and Valente, A. (2018d). Compression of electrocardiographs comparative study between the walsh hadamard transform and discrete cosine transform.
- Saraiva, A. A., N. F. F., Salviano F.S.P. Soares and, M. J. C. S. R., and Antonio, V. (2018e). Filtering of cardiac signals with mathematical morphology for qrs detection. *Proceedings of ICAT'18, 7th International Conference on Advanced Technologies*.
- Saraiva, A. A., Costa, N., Sousa, J. V. M., De Araujo, T. P., Ferreira, N. F., and Valente, A. (2018f). Scalable task cleanup assignment for multi-agents. In *Memorias de Congressos UTP*, volume 1, pages 439–446.
- Saraiva, A. A., Nogueira, A. T., Ferreira, N. F., and Valente, A. (2018g). Application of virtual reality for the treatment of strabismus and amblyopia. In *2018 IEEE 6th International Conference on Serious Games and Applications for Health (SeGAH)*, pages 1–7. IEEE.
- Saraiva, A. A., SANTOS, D. S., JUNIOR, F. M., SOUSA, J. V. M., FERREIRA, N. F., and Valente, A. (2018h). Navigation of quadruped multirobots by gesture recognition using restricted boltzmann machines. In *Memorias de Congressos UTP*, volume 1, pages 431–438.
- Sivaramakrishnan, R., Antani, S., Xue, Z., Candemir, S., Jaeger, S., and Thoma, G. (2017). Visualizing abnormalities in chest radiographs through salient network activations in deep learning. In *Life Sciences Conference (LSC), 2017 IEEE*, pages 71–74. IEEE.
- Tang, J., Deng, C., and Huang, G.-B. (2016). Extreme learning machine for multilayer perceptron. *IEEE transactions on neural networks and learning systems*, 27(4):809–821.
- Ustinova, E., Ganin, Y., and Lempitsky, V. (2017). Multi-region bilinear convolutional neural networks for person re-identification. In *Advanced Video and Signal Based Surveillance (AVSS), 2017 14th IEEE International Conference on*, pages 1–6. IEEE.
- Vajda, S., Karargyris, A., Jaeger, S., Santosh, K., Candemir, S., Xue, Z., Antani, S., and Thoma, G. (2018). Feature selection for automatic tuberculosis screening in frontal chest radiographs. *Journal of medical systems*, 42(8):146.
- Vehtari, A., Gelman, A., and Gabry, J. (2017). Practical bayesian model evaluation using leave-one-out cross-validation and waic. *Statistics and Computing*, 27(5):1413–1432.
- Wang, X., Peng, Y., Lu, L., Lu, Z., Bagheri, M., and Summers, R. M. (2017). Chestx-ray8: Hospital-scale chest x-ray database and benchmarks on weakly-supervised classification and localization of common thorax diseases. In *Computer Vision and Pattern Recognition (CVPR), 2017 IEEE Conference on*, pages 3462–3471. IEEE.
- Xue, Z., Antani, S., Long, L. R., and Thoma, G. R. (2018). Using deep learning for detecting gender in adult chest radiographs. In *Medical Imaging 2018: Imaging Informatics for Healthcare, Research, and Applications*, volume 10579, page 105790D. International Society for Optics and Photonics.
- Yu, S., Jia, S., and Xu, C. (2017). Convolutional neural networks for hyperspectral image classification. *Neurocomputing*, 219:88–98.